Inorganic Chemistry

Article

pubs.acs.org/IC

Efficient Light Harvesting and Energy Transfer in a Red Phosphorescent Iridium Dendrimer

Yang-Jin Cho,[†] Seong Ahn Hong,[†] Ho-Jin Son,*[,†] Won-Sik Han,*[,‡] Dae Won Cho,*[,†] and Sang Ook Kang*[,†]

[†]Department of Advanced Materials Chemistry, Korea University, Sejong 339-700, South Korea

[‡]Department of Chemistry, Seoul Women's University, Seoul 139-774, South Korea

Supporting Information

ABSTRACT: A series of red phosphorescent iridium dendrimers of the type [Ir(btp)$_2$(pic-PC$_n$)] (**Ir-G$_n$**; n = 0, 1, 2, and 3) with two 2-(benzo[b]thiophen-2-yl)pyridines (btp) and 3-hydroxypicolinate (pic) as the cyclometalating and ancillary ligands were prepared in good yields. Dendritic generation was grown at the 3 position of the pic ligand with 4-(9H-carbazolyl)phenyl dendrons connected to 3,5-bis(methyleneoxy)benzyloxy branches (PC$_n$; n = 0, 2, 4, and 8). The harvesting photons on the PC$_n$ dendrons followed by efficient energy transfer to the iridium center resulted in high red emissions at ∼600 nm by metal-to-ligand charge transfer. The intensity of the phosphorescence gradually increased with increasing dendrimer generation. Steady-state and time-resolved spectroscopy were used to investigate the energy-transfer mechanism. On the basis of the fluorescence quenching rate constants of the PC$_n$ dendrons, the energy-transfer efficiencies for **Ir-G$_1$**, **Ir-G$_2$**, and **Ir-G$_3$** were 99, 98, and 96%, respectively. The energy-transfer efficiency for higher-generation dendrimers decreased slightly because of the longer distance between the PC dendrons and the core iridium(III) complex, indicating that energy transfer in **Ir-G$_n$** is a Förster-type energy transfer. Finally, the light-harvesting efficiencies for **Ir-G$_1$**, **Ir-G$_2$**, and **Ir-G$_3$** were determined to be 162, 223, and 334%, respectively.

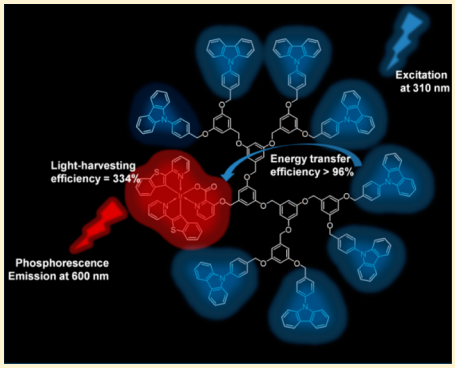

INTRODUCTION

Organic light-emitting diodes (OLEDs) have attracted much attention as next-generation full-color displays and lighting sources owing to their many advantages such as excellent performance and easy fabrication.[1,2] The phosphorescence transition-metal complexes have attracted particular interest because they utilize both singlet and triplet excitons, which theoretically enables 100% internal quantum efficiencies.[3] Furthermore, a number of solution-processable phosphorescent polymers[4,5] as well as dendrimers,[6−9] have been prepared. In particular, iridium-cored dendrimers have many advantages such as (i) long-lived excited states and high luminescence efficiency,[10] (ii) suitable solubility for solution-processable phosphorescent OLEDs,[11−13] (iii) reduction of strong interactions between the emitting phosphors under high current density such as triplet−triplet annihilation,[14−16] and (iv) prevention of the quenching of luminescence by site isolation and shielding of the iridium core to impede oxygen quenching.[17] In this regard, the energy-transfer mechanism for blue-emitting divergent iridium dendrimers with the peripheral phenylcarbazole units has been reported.[18,19] Efficient energy transfer was observed by the enhancement of blue phosphorescence efficiencies with increasing peripheral phenylcarbazole units.

In general, red-emitting iridium complexes exhibit low quantum yields compared to green and blue phosphorescent iridium complexes because of the decreasing energy difference between the excited and ground states, causing a lapse of excited-state energy by the radiationless deactivation pathway, namely, an increase in the nonradiative rates (k_{nr}) and a decrease in the radiative rates (k_r) for longer-wavelength emission, resulting in a lower quantum efficiency for red emitters. Therefore, the development of highly efficient red-emitting materials is very important. Within the scope of light harvesting and energy transfer for the same Ir-PC dendrons, we have focused on the color rendering to red by employing 2-(benzo[b]thiophen-2-yl)pyridine (btp) cyclometalating ligands. Although there are many reports of red-emitting iridium-based-dendrimer systematic studies on light harvesting and energy transfer,[20−24] studies on the red-emitting materials and clarification of their emissive mechanism are scarce.

In this study, we investigated the detailed energy-transfer mechanism of red-emitting divergent iridium dendrimers. As red-emitting dendrimers, we synthesized new dendritic complexes Ir(btp)$_2$(pic-PC$_2$) (**Ir-G$_1$**), Ir(btp)$_2$(pic-PC$_4$) (**Ir-G$_2$**), Ir(btp)$_2$(pic-PC$_8$) (**Ir-G$_3$**), and reference complex Ir(btp)$_2$(pic-OH) (**Ir-G$_0$**), where btp = 2-(benzo[b]thiophen-2-yl)pyridine, pic = picolinate, and PC$_n$ = 4-(9H-carbazolyl)-phenylcarbazole dendrons (n = 0, 2, 4, and 8), as shown in Chart 1. The btp ligand was introduced because the Ir(btp)$_2$(acac) complex is known to emit red phosphorescence

Received: September 24, 2014
Published: November 24, 2014

   dx.doi.org/10.1021/ic502323w | Inorg. Chem. 2014, 53, 13136−13141

Chart 1. Molecular Structures of Red-Emitting Ir-G$_n$ (n = 0, 1, 2, and 3) Dendrimers

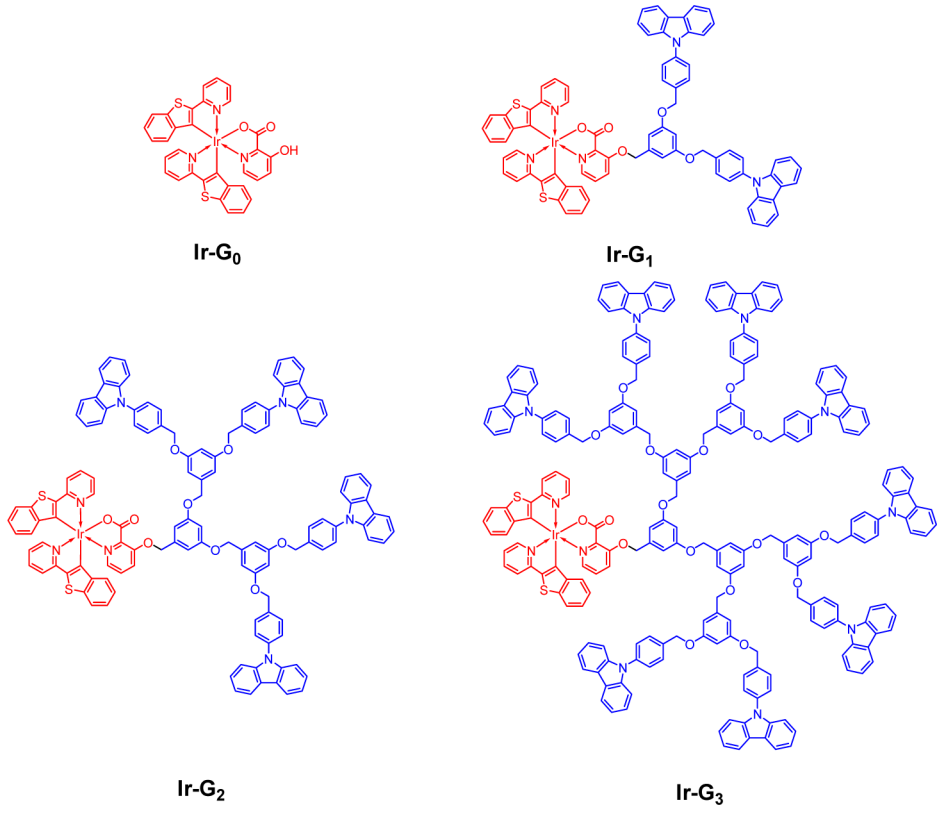

at 612 nm.[24−23] The PC$_n$ units were introduced at the 3 position of the picolinate ligand via 3,5-bis(methyleneoxy)-benzyloxy branches. The as-prepared dendrimers comprising the PC$_n$ dendrons, 3,5-bis(methyleneoxy)benzyloxy, and Ir(btp)$_2$(pic) as the light-harvesting and donor unit, branching unit, and acceptor unit established an efficient energy-transfer system, leading to a highly luminescent red phosphorescent. Even though btp-based iridium(III) dendrimers with carbazoyl dendrons were reported previously,[30] their detailed photodynamics were not reported. Herein, we studied the relationship between the light-harvesting and energy-transfer efficiencies using quantitative kinetic analysis of the steady-state absorption, energy transfer in the excited state, fluorescence data, and time-resolved fluorescence data.

EXPERIMENTAL SECTION

General Information. All compounds were synthesized in a dry dinitrogen atmosphere. Dichloromethane (CH_2Cl_2), acetonitrile (CH_3CN), and dimethylformamide were distilled from calcium hydride. Tetrahydrofuran (THF) was distilled from sodium/benzophenone under a dinitrogen atmosphere. All solvents were stored over molecular sieves. Other reagents were obtained commercially and used without further purification. Glassware, syringes, magnetic stirring bars, and needles were dried in a convection oven for over 4 h. Reactions were checked with thin-layer chromatography (TLC; Merck Co.). The spots developed onto TLC were identified under UV light at 254 and 365 nm. Column chromatography was done on silica gel 60 G (particle size 5−40 μm; Merck Co.). Synthesized compounds were characterized by ^{1}H and ^{13}C NMR and high-resolution mass spectrometry (HR-MS) (fast atom bombardment, FAB) or matrix-assisted laser desorption ionization time-of-flight (MALDI-TOF) mass analysis. The ^{1}H and ^{13}C NMR spectra were recorded on a Varian Mercury 300 spectrometer operated at 300.1 and 75.4 MHz, respectively. The HR-MS (FAB) (Jeol Ltd. JMS-HX 110/110A), electrospray ionization mass spectrometry (ESI-MS; Waters Synapt G2 HDMS quadrupole TOF mass spectrometer equipped with an ESI source), and MALDI-TOF mass spectroscopy (ABI Voyager STR) were performed by the Ochang branch of the Korean Basic Science Institute.

Caution! *All procedures involving $IrCl_3{\cdot}H_2O$ were carried out in an inert atmosphere despite the air stability of the compounds, with the main concern being the oxidative and thermal stability of intermediate complexes at the high temperatures used in the reactions.*

Cyclometalated Ir^{3+}-μ-chloro-bridged dimers of the general formula $[(btp)_2Ir(\mu\text{-}Cl)]_2$[31] and PC$_n$-Br dendrons[18] were synthesized by previously reported methods.

Iridium(III) Bis[2-(2′-benzothienyl)pyridinato-*N*,*C*$^{3'}$]-3-hydroxypicolinate, Ir(btp)$_2$(pic-OH) (Ir-G$_0$). A mixture of the crude $[(btp)_2Ir(\mu\text{-}Cl)]_2$ (0.48 g, 0.4 mmol), 3-hydroxypicolinic acid (0.16 g, 1.2 mmol), and sodium carbonate (0.33 g, 3.1 mmol) was dissolved in 2-ethoxyethanol (25 mL) and heated to 120 °C for 15 h. After cooling to room temperature, the mixture was quenched with water. The organic phase was extracted with CH_2Cl_2 and then dried over $MgSO_4$. After removal of the solvents under reduced pressure, the residue was purified by silica gel column chromatography using CH_2Cl_2/methanol (100:1, v/v) as an eluent to give the desired product (yield: 0.9 g, 65%). ^{1}H NMR (300.1 MHz, $CDCl_3$): δ 13.56 (s, 1H), 8.76 (d, J = 5.7 Hz, 1H), 7.80−7.73 (m, 3H), 7.68−7.62 (m, 3H), 7.43−7.38 (m, 2H), 7.20−7.15 (m, 3H), 7.11−7.06 (m, 2H), 6.90−6.86 (m, 2H), 6.79 (t, J = 7.2 Hz, 1H), 6.26 (d, J = 8.1 Hz, 1H), 6.00 (d, J = 8.1 Hz, 1H). ^{13}C NMR (75.4 MHz, $CDCl_3$): δ 178.1, 166.6, 165.1, 160.7, 149.8, 149.1, 147.4, 146.7, 145.7, 144.0, 142.8, 142.7, 140.8, 138.9, 138.6, 136.5, 134.7, 134.6, 130.3, 127.4, 125.8, 125.5, 125.2, 124.3, 123.9, 123.2, 123.0, 120.0, 119.4, 118.7. ESI-MS: m/z 751.0583 (calcd for $[M + H]^+$: m/z 751.0575).

Ir(btp)$_2$(pic-PC$_n$) (Ir-G$_n$). A mixture (3:1, v/v) of PC$_n$-Br (0.27 mmol), Ir(btp)$_2$(pic-OH) (0.27 mmol), and K_2CO_3 (0.3 g, 2.17 mmol) in CH_3CN (12 mL) and THF (4 mL) was refluxed under a dinitrogen environment for 12 h. The details of the synthesis of PC$_n$-Br have been described previously.[18] After cooling to room

dx.doi.org/10.1021/ic502323w | Inorg. Chem. 2014, 53, 13136−13141

temperature, the reaction mixture was poured into water. The organic phase was extracted with CH_2Cl_2 and dried over $MgSO_4$. After removal of the solvents under reduced pressure, the residue was purified by silica gel column chromatography, eluting with CH_2Cl_2 to remove PC_n-Br and then CH_2Cl_2/ethyl acetate [1:1 (v/v) for **Ir-G$_1$**, 1:4 for **Ir-G$_2$**, and 1:5 for **Ir-G$_3$**] to provide the desired product as a white solid (yield: 80% for **Ir-G$_1$**, 57% for **Ir-G$_2$**, and 24% for **Ir-G$_3$**).

Ir-G$_1$. ^{1}H NMR (300.1 MHz, $CDCl_3$): δ 8.92 (d, J = 5.6 Hz, 1H), 8.16 (d, J = 7.7 Hz, 3H), 7.75−7.56 (m, 14H), 7.42−7.39 (m, 10H), 7.33−7.28 (m, 6H), 7.21−7.01 (m, 6H), 6.84 (t, J = 7.4 Hz, 1H), 6.76 (t, J = 7.2 Hz, 2H), 6.70 (s, 1H), 6.26 (d, J = 8.1 Hz, 1H), 5.97 (d, J = 8.1 Hz, 1H), 5.33 (s, 2H), 5.21 (s, 4H). ^{13}C NMR (75.4 MHz, $CDCl_3$): δ 165.3, 160.5, 160.4, 146.1, 143.0, 142.7, 141.0, 138.7, 138.5, 137.6, 136.2, 129.5, 129.4, 129.3, 127.4, 127.3, 126.2, 125.9, 125.7, 125.1, 124.2, 123.1, 122.9, 120.5, 120.2, 119.8, 119.7, 119.3, 118.5, 110.0, 105.7, 70.0. MALDI-TOF: m/z 1384.363 (calcd for $[M + H]^+$: m/z 1383.3039).

Ir-G$_2$. ^{1}H NMR (300.1 MHz, $CDCl_3$): δ 8.87 (d, J = 5.6 Hz, 1H), 8.14 (d, J = 7.7 Hz, 10H), 7.72−7.54 (m, 23H), 7.40−7.37 (m, 22H), 7.30−7.28 (m, 6H), 7.00−6.62 (m, 12H), 6.23 (d, J = 7.7 Hz, 1H), 5.94 (d, J = 8.0 Hz, 1H), 5.19 (s, 2H), 5.17 (s, 8H), 5.09−5.07 (m, 4H). ^{13}C NMR (75.4 MHz, $CDCl_3$): δ 160.4, 160.3, 141.0, 139.8, 137.7, 137.6, 136.2, 136.1, 129.9, 129.3, 127.4, 126.2, 123.6, 120.5, 120.2, 110.0, 106.9, 105.7, 102.0, 70.2, 70.0. MALDI-TOF: m/z 2138.691 (calcd for $[M + H]^+$: m/z 2137.5871).

Ir-G$_3$. ^{1}H NMR (300.1 MHz, $CDCl_3$): δ 8.84 (d, J = 5.5 Hz, 1H), 8.12 (d, J = 7.2 Hz, 18H), 7.61−7.59 (m, 16H), 7.55−7.54 (m, 26H), 7.44 (s, 4H), 7.37 (m, 44H), 6.89−6.64 (m, 23H), 5.12−5.10 (m, 16H), 5.02 (s, 12H), 4.93 (m, 6H). ^{13}C NMR (75.4 MHz, $CDCl_3$): δ 160.3, 141.0, 139.7, 137.7, 136.1, 130.3, 129.3, 127.3, 126.2, 126.0, 123.6, 123.4, 120.5, 120.2, 119.9, 109.9, 106.8, 101.9, 70.2, 69.9. MALDI-TOF: m/z 3646.657 (calcd for $[M + H]^+$: m/z 3646.1534).

Steady-State Absorption and Fluorescence Measurements. Absorption spectra were recorded on a Shimadzu (UV-3101PC) scanning spectrophotometer. Emission and excitation spectra were measured using a Varian fluorescence spectrophotometer (Cary Eclipse).

Phosphorescence Measurements. In order to excite the carbazole dendron, a 309 nm pulse was generated by using a H_2−Raman shifter using the third harmonic (355 nm) of a Q-switched Nd:YAG laser (Continuum, Surelite II; pulse width of 4.5 ns). The phosphorescence spectra were recorded by an ICCD detector (Andor, iStar) equipped to a monochromator (DongWoo Optron, Monora 500i). The temporal profiles were measured using a monochromator equipped with a photomultiplier (Zolix Instruments Co., CR 131) and a digital oscilloscope (Tektronix, TDS-784D). All sample solutions were argon-saturated to remove oxygen. The fluorescence lifetime was measured using a single-photon-counting method with a streak scope (Hamamatsu Photonics, C10627-03) equipped with a polychromator (Acton Research, SP2300). An ultrashort laser pulse was generated with a Ti:sapphire oscillator (Coherent, Vitesse; fwhm 100 fs) pumped with a diode-pumped solid-state laser (Coherent, Verdi). High-power (1.5 mJ) pulses were generated using a Ti:sapphire regenerative amplifier (Coherent, Libra; 1 kHz). The pulse (330 nm) generated from an optical parametric amplifier (Coherent, TOPAS) was used as the excitation pulse. The temporal emission profiles were well-fitted to a single-exponential function. The time resolution was approximately 20 ps after the deconvolution procedure. The goodness of fit was judged by weighted residuals and the χ^2 values.

Transient Absorption (TA) Measurements. The nanosecond TA measurements were conducted using laser flash photolysis.[32] The samples were excited by third-harmonic generation (355 nm, fwhm of 4.5 ns) from a Q-switched Nd:YAG laser (Continuum, Surelite II-10). Light from a xenon arc lamp (ILC Technology, PS 300-1) was focused on the sample for the TA measurements. Temporal profiles were measured with a monochromator (DongWoo Optron, Monora 500i) equipped with a fast photomultiplier tube (Zolix Instruments Co., CR 131) and a digital oscilloscope (Tektronix, TDS-784D). The reported signals were averaged for 600 events to obtain satisfactory signal-to-noise ratios. The TA spectra were measured with an intensified charge-coupled device (Ando, iStar).

RESULTS AND DISCUSSION

Absorption and Emission Properties of Ir-G$_0$ and Ir-G$_n$. Figure 1 shows the absorption spectra of **Ir-G$_n$** in CH_2Cl_2. The

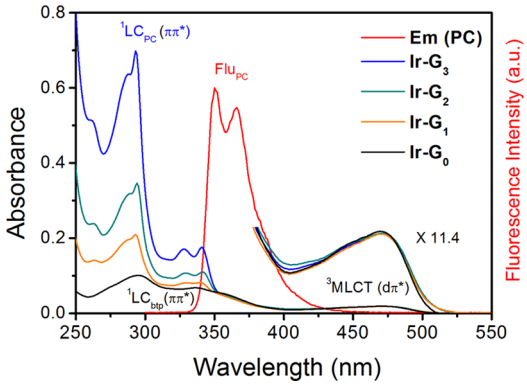

Figure 1. Absorption spectra of **Ir-G$_0$** and **Ir-G$_n$** in a 4 μM solution in CH_2Cl_2. The red fluorescence spectrum corresponds to PC in CH_2Cl_2 (λ_{ex} = 290 nm).

reference complex **Ir-G$_0$** shows a strong absorption band at 300 nm, attributed to the spin-allowed btp-ligand-centered (^{1}LC, $\pi \rightarrow \pi^*$) transitions. The absorption band at 475 nm was assigned to the spin-forbidden metal-to-ligand charge-transfer (^{3}MLCT, dπ^*) transition.

The absorption spectra of **Ir-G$_n$** (n = 1, 2, and 3) show the characteristic absorption bands for the PC dendron at 293 nm ($^1L_a \leftarrow {}^1A$ transition) and 340 nm ($^1L_b \leftarrow {}^1A$ transition).[33,34] The absorbance of these bands increased proportionally with increasing number of PC units in the dendron, but the shape of the spectra was not changed, indicating that there is no significant electronic interaction between the PC_n donor and the iridium(III) core acceptor in the ground state. While the absorption intensities of ^{1}LC at ∼300 nm are proportional to the increasing number of PC units, the absorption intensities of the ^{3}MLCT absorption bands of **Ir-G$_n$** at ∼470 nm were not changed according to increasing dendrimer generation, as shown in the enlarged inset of Figure 1. Notably, the fluorescence spectrum of [4-(9*H*-carbazol-9-yl)phenyl]-methanol (PC) in the region ∼330−450 nm is well overlapped with the ^{1}LC absorption band of the btp ligand (or partially MLCT) of **Ir-G$_n$**, in which induced Förster-type energy transfer from the excited singlet PC_n chromophores to the iridium(III) center in the excited singlet manifold (vide infra) occurred.

In the emission spectrum at 298 K, **Ir-G$_0$** shows the characteristic phosphorescence emission at 600 and 650 nm, as shown in Figure 2. At 77 K, the emission spectrum of **Ir-G$_0$** in 2-MeTHF exhibits vibrational structures at 590 and 650 nm ($\Delta\nu$: ∼1565 cm^{-1}, the C=C stretching mode of the aromatic ring) and is slightly blue-shifted compared to that at 298 K. With increasing number of PC dendrons in **Ir-G$_n$**, a gradual enhancement in red phosphorescence was observed, whereas the fluorescence from PC dendrons was markedly quenched compared to those of the PC_n dendrons measured under identical conditions (Figure S1 in the Supporting Information, SI). This result indicates that an efficient energy transfer occurred from the excited singlet state of the PC_n dendrons to the iridium(III) center followed by radiative decays from the

dx.doi.org/10.1021/ic502323w | Inorg. Chem. 2014, 53, 13136−13141

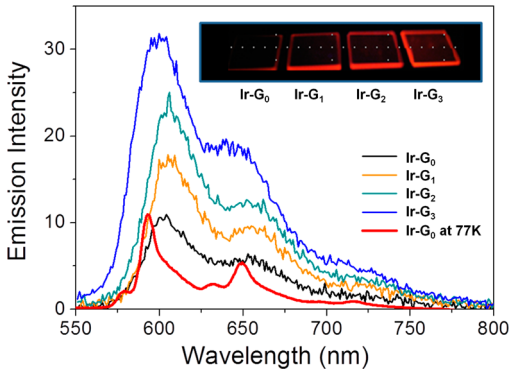

Figure 2. Emission spectra of **Ir-G$_0$** and **Ir-G$_n$** in a 4 μM solution in CH_2Cl_2 at 298 K. The red spectrum of **Ir-G$_0$** was measured in 2-MeTHF at 77 K. All emission spectra were excited at 290 nm. Inset: emission of **Ir-G$_n$** films with PMMA under illumination at 320 nm, which are coated onto a quartz plate.

iridium(III) center. Therefore, the PC$_n$ dendrons successfully encapsulated the iridium(III) center without a direct effect on the energy state and/or excited state of the iridium(III) center. The inset in Figure 2 shows red phosphorescence of 200 μmol of **Ir-G$_0$** and **Ir-G$_n$** in a poly(methyl methacrylate) (PMMA) film under illumination at 320 nm. Although the same amount of the core iridium complex was included in each sample, the red emissions were enhanced gradually with increasing dendrimer generation. This is visual evidence for light harvesting in **Ir-G$_n$**.

Quenching Efficiencies and Rate Constants of Energy Transfer Using an Emission Lifetime. The fluorescence lifetimes monitored at 350 nm for the PC$_n$-OH dendrons (n = 2, 4, and 8; structures are shown in Figure S1 in the SI) were measured as 6.1 ns.[18] In contrast, the fluorescence lifetimes monitored at 350 nm remarkably decreased when the PC$_n$ dendrons were attached to the picolinate ancillary ligand of the Ir(btp)$_2$(pic) complex via 3,5-bis(methyleneoxy)benzyloxy branches, and this can be explained by efficient energy transfer from the PC$_n$ dendrons to the iridium(III) center. The measured fluorescence lifetimes for **Ir-G$_1$**, **Ir-G$_2$**, and **Ir-G$_3$** were 0.08, 0.15, and 0.25 ns, respectively. Notably, small contributions of longer-lifetime components (~6 ns) were observed, arising from the unquenched residual fraction of the excited PC dendrons.

The phosphorescence lifetimes of **Ir-G$_n$** upon excitation at 309 nm and monitoring at 593 nm did not change accordingly to 8.4 and 10.3 μs at 298 K (in CH_2Cl_2) and 77 K (in 2-MeTHF), respectively, as shown in Figure S2 (see the SI). The phosphorescence lifetimes for **Ir-G$_n$** are listed in Table 1. Although the PC$_n$ dendrons dominantly absorb the excitation light of 309 nm, the enhanced phosphorescence of the core iridium complex and fluorescence quenching of the PC$_n$ dendrons in **Ir-G$_n$** indicate that the final emitting states of **Ir-G$_n$** are the ^{3}LC and ^{1,3}MLCT mixed states of the iridium(III) center.

On the basis of the fluorescence decay time constants, the energy-transfer efficiencies of the dendrimers were estimated using the following equation,[35,36] corresponding to the fluorescence quenching efficiencies:

$$\varepsilon_q\ (\%) = \left(1 - \frac{\tau_{AD}}{\tau_D}\right) \times 100 \qquad (1)$$

Table 1. Lifetimes of Fluorescence (τ_f) and Phosphorescence (τ_p) at Room Temperature and 77 K

	τ_f (ns)	τ_p (μs)	
complex	298 K[a]	298 K[b]	77 K[c]
Ir-G$_0$		8.3	10.6
Ir-G$_1$	0.08	8.1	10.1
Ir-G$_2$	0.15	8.4	10.2
Ir-G$_3$	0.25	8.8	10.0
PC$_8$-OH	6.13		

[a]Monitored at 380 nm in a CH_2Cl_2 solution. [b]Monitored at 600 nm in a CH_2Cl_2 solution. [c]Monitored at 593 nm in a 2-MeTHF matrix. All decay profiles were excited at 309 nm.

where τ_D and τ_{AD} are the fluorescence lifetimes of the PC$_n$ dendrons in the absence and presence of the acceptor iridium(III) center. The fluorescence quenching efficiencies (ε_q) are determined as 99, 98, and 96% for **Ir-G$_1$**, **Ir-G$_2$**, and **Ir-G$_3$**, respectively. High ε_q values indicate that the excited PC$_n$ is deactivated by an efficient energy transfer to the ^{1}MLCT state followed by the ^{3}MLCT and/or ^{3}LC states of the iridium(III) center. ε_q in high generations, **Ir-G$_2$** and **Ir-G$_3$**, slightly decreased because of the longer distance between the PC dendrons and the core iridium(III) complex, indicating that energy transfer in **Ir-G$_n$** is a Förster-type energy transfer.

Because the fluorescence lifetimes of the PC$_n$ dendrons in **Ir-G$_n$** were clearly decreased by introduction of the iridium(III) center, the quenching rate can be estimated accordingly using an energy-transfer rate constant (k_{ET}), and k_{ET} can be determined experimentally using the following equation:[37]

$$k_{ET} = \frac{1}{\tau_D}\left(\frac{1}{\frac{1}{\phi_{ET}} - 1}\right) \qquad (2)$$

where τ_D is the fluorescence lifetime of the donor in the absence of the acceptor (Table 1) and ϕ_{ET} is the energy-transfer efficiency. These values can be applied to the fluorescence quenching efficiencies (ε_q) of the PC$_n$ dendrons of each generation determined using eq 1. Using eq 2, k_{ET} values of the dendrimers were estimated to be 1.3×10^{10}, 6.4×10^9, and 3.8×10^9 s^{-1} for **Ir-G$_1$**, **Ir-G$_2$**, and **Ir-G$_3$**, respectively, as listed in Table 2.

Energy-Transfer Mechanism. Energy transfer in **Ir-G$_n$** follows the Förster energy-transfer mechanism. A Förster

Table 2. Quenching Efficiency, Phosphorescence Harvesting Efficiency, Experimental and Calculated Energy-Transfer Rate Constants (k_{ET}), and Average Distances (R_{DA}) between the Donor and Acceptor Estimated by Semiempirical Calculations and the Förster Distances (R_F) of Ir-G$_n$

	quenching efficiency (%)	light-harvesting iridium core (%)[a]	k_{ET}(exp) (s^{-1})	k_{ET}(cal) (s^{-1})	R_{DA} (Å)	R_F (Å)
Ir-G$_1$	99	162 (159)	1.3×10^{10}	1.4×10^{10}	16	34
Ir-G$_2$	98	223 (217)	6.4×10^9	7.3×10^9	19	36
Ir-G$_3$	96	334 (330)	3.8×10^9	4.0×10^9	21	36

[a]Using reference to **Ir-G$_0$**. The values in parentheses are determined by eq 5.

dx.doi.org/10.1021/ic502323w | Inorg. Chem. 2014, 53, 13136−13141

distance (R_F) is the distance at which resonance energy transfer is 50% efficient, and R_F can be calculated using the following equation:[38]

$$R_F^6 = \frac{9000(\ln 10)\phi_D k^2}{128\pi^5 N n^4} J, \qquad J = \int_0^\infty f_D(\lambda)\,\varepsilon(\lambda)\,\lambda^4\,d\lambda \tag{3}$$

where ϕ_D is the fluorescence quantum yield of the donor (=0.3), N is Avogadro's number, κ^2 is the orientation factor of the transition dipole moments ($=^2/_3$), n is the index of refraction in CH_2Cl_2 (1.4246), J is the overlap integral of the normalized donor emission spectrum (f_D) with the acceptor molar extinction coefficient (ε), which results in 4.92×10^{-14} M^{-1} cm^3 for all dendrimers. R_F calculated in accordance to eq 3 was in the range 3.4−3.6 nm for **Ir-G$_n$** and is in the typical distance range (1−10 nm) for long-range interaction in the Förster mechanism. Therefore, we can conclude that energy transfer from the PC$_n$ dendrons to the iridium(III) center occurred by the Förster mechanism.

The energy-transfer rate constant can be determined by the Förster model, as represented by the following equation:

$$k_{ET} = \frac{1}{\tau_D}\left(\frac{R_F}{R_{DA}}\right)^6 \tag{4}$$

where τ_D is the fluorescence lifetime (6.1 ns) of the donor in the absence of the acceptor and R_{DA} is the distance between the donor and acceptor moieties. The average distances between the PC$_n$ dendrons and the btp main ligand (R_{DA} are 16, 19, and 21 Å) were adapted for the three **Ir-G$_n$**, which were calculated from the energy-minimized geometries from many computer-generated conformers using semiempirical calculation (the PM3 method),[39] and their molecular geometries are shown in Figure S4 in the SI. Using these average distance values, the k_{ET} values were calculated to be 1.4×10^{10} (**Ir-G$_1$**), 7.3×10^9 (**Ir-G$_2$**), and 4.0×10^9 s^{-1} (**Ir-G$_3$**), which agree well with the experimental results, as listed in Table 2.

Light-Harvesting Efficiency. Figure 2 shows that the intensities of phosphorescence in **Ir-G$_n$** gradually increased compared to that of **Ir-G$_0$** even though each dendrimer has only one iridium center. Because their fluorescence quenching efficiencies are almost quantitative for **Ir-G$_{1-3}$**, gradual enhancement in the phosphorescence is easily explained by the light-harvesting efficiency. The actual enhancement in phosphorescence can be calculated by the ratio of $I_P/I_P^0 \times 100$, where I_P and I_P^0 are integrated phosphorescence intensities of the iridium complex in the presence and absence of donors, respectively. As listed in Table 2, the phosphorescence enhancements of the core iridium complex are 162%, 223%, and 334% for **Ir-G$_1$**, **Ir-G$_2$**, and **Ir-G$_3$**, respectively.

The light harvesting depends on the energy-transfer efficiency and emission quantum yield of the donor. Therefore, the light-harvesting efficiency (ε_{LH}) is represented by the following equation:[18]

$$\varepsilon_{LH}\,(\%) = (1 + n\phi_{ET}\phi_f) \times 100 \tag{5}$$

where n is the number of PC units in the dendrons, ϕ_{ET} is the energy-transfer efficiency (same value as the fluorescence quenching efficiency) in the range of 0.96−0.98, and ϕ_f is the fluorescence quantum yield (ϕ_f = 0.3) of the donor PC$_n$-OH. The calculated light-harvesting efficiencies using this relationship showed good agreement with the experimental values, as shown in Table 2.

TA Study. Nanosecond laser flash photolysis experiments were performed at room temperature to confirm the photodynamics of the excited state of **Ir-G$_n$**. The TA spectra were collected at 100 ns delay after excitation at 309 nm. Figure 3 shows the TA spectra of **Ir-G$_0$** and **Ir-G$_1$** in argon-saturated CH_2Cl_2 measured under identical conditions. The TA spectra of **Ir-G$_2$** and **Ir-G$_3$** are shown in Figure S5 in the SI. All of the TA spectra of **Ir-G$_n$** showed basically identical spectral features.

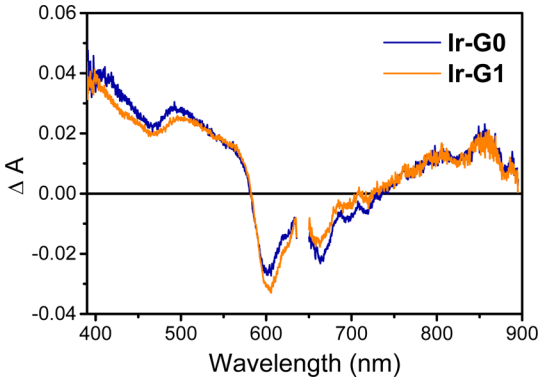

Figure 3. TA spectra of **Ir-G$_0$** and **Ir-G$_1$** measured at 100 ns delay after excitation at 309 nm in argon-saturated CH_2Cl_2 as obtained by the laser flash photolysis technique.

The TA spectrum of **Ir-G$_0$** exhibited the typical features of a charge-transfer state of the core iridium complex. The strong and broad bands in the range 400−500 nm were assigned to the formation of a radical anion of the btp ligand, which may be formulated as $Ir^{4+}(btp^{\bullet 1/2-})_2$(pic-Ph) via the MLCT process. The similarity between the transient spectra of **Ir-G$_0$** and **Ir-G$_n$** indicates that the lowest excited state (emissive state) is the MLCT state. Any other new transient spectral features relating to the cationic radical of the PC$_n$ dendrons were not observed, indicating that energy transfer occurred via the Förster mechanism, not electron transfer.

CONCLUSIONS

A series of red-emissive Ir(btp)$_2$(pic-PC$_n$) dendrimers comprising the PC$_n$ dendrons, 3,5-bis(methyleneoxy)benzyloxy, and Ir(btp)$_2$(pic) as the light-harvesting and donor unit, branching unit, and acceptor unit, respectively, were synthesized and established as an efficient energy-transfer system, leading to highly luminescent red phosphorescence. The excited-state energy of the PC$_n$ dendrons was exothermically transferred to the iridium center. Moreover, fluorescence of the PC$_n$ dendrons overlapped well with the ^{1}LC* absorption band of the btp ligand and partially with the ^{3}MLCT band. Therefore, energy transfer can be explained by the Förster model. The energy-transfer efficiencies for **Ir-G$_n$** were quantitative, albeit a slight decrease was observed in the high-generation dendrimers because of the longer distance between the donor and acceptor. The energy-transfer rate constants calculated by the Förster model showed a good agreement with the experimental values, indicating that the relationship for the enhancement in light harvesting strongly depends on key factors such as the number of PC dendrons, fluorescence quantum yield of PC$_n$, and energy-transfer efficiency. As a result, the light-harvesting efficiencies of 162% (**Ir-G$_1$**), 233% (**Ir-G$_2$**), and 334% (**Ir-G$_3$**) were determined.

dx.doi.org/10.1021/ic502323w | Inorg. Chem. 2014, 53, 13136−13141

■ ASSOCIATED CONTENT

Supporting Information

Emission spectra of free PC_n-dendrons and **Ir-G$_n$**, phosphorescence decay profiles of **Ir-G$_n$** at 298 K (in CH_2Cl_2) and 77 K (in 2-MeTHF), emission spectra of **Ir-G$_n$** at 77 K in 2-MeTHF, molecular geometries of **Ir-G$_n$** calculated by the PM3 method, and TA spectra of **Ir-G$_2$** and **Ir-G$_3$**. This material is available free of charge via the Internet at http://pubs.acs.org.

■ AUTHOR INFORMATION

Corresponding Authors

*E-mail: hjson@korea.ac.kr.
*E-mail: wshan@swu.ac.kr.
*E-mail: dwcho@korea.ac.kr.
*E-mail: sangok@korea.ac.kr.

Notes

The authors declare no competing financial interest.

■ ACKNOWLEDGMENTS

This research was supported by the Basic Science Research Program through the National Research Foundation of Korea, funded by the Ministry of Education (Grant 2014R1A6A1030732). This work was also supported by the Korea Evaluation Institute of Industrial Technology, funded by the Ministry of Knowledge Economy (Korea) through the Improving Competitiveness of Materials and Components Industry Program (Grant 10042682). We also acknowledge the Chungcheong Institute for Regional Program Evaluation (Grant A0046 00226).

■ REFERENCES

(1) Tang, C. W.; Van Slyke, S. A.; Chen, C. H. *J. Appl. Phys.* **1989**, *65*, 3610−3616.
(2) Tsutsui, T.; Takada, N. *Jpn. J. Appl. Phys.* **2013**, *52*, 110001.
(3) Baldo, M. A.; O'Brien, D. F.; You, Y.; Shoustikov, A.; Sibley, S.; Thompson, M. E.; Forrest, S. R. *Nature* **1998**, *395*, 151−154.
(4) Sandee, A. J.; Williams, C. K.; Evans, N. R.; Davies, J. E.; Boothby, C. E.; Köhler, A.; Friend, R. H.; Holmes, A. B. *J. Am. Chem. Soc.* **2004**, *126*, 7041−7048.
(5) Jiang, J.; Jiang, C.; Yang, W.; Zhen, H.; Huang, F.; Cao, Y. *Macromolecules* **2005**, *38*, 4072−4080.
(6) Ding, J.; Lű, J.; Cheng, Y.; Xie, Z.; Wang, L.; Jing, X.; Wang, F. *Adv. Funct. Mater.* **2008**, *18*, 2754−2762.
(7) Ding, J.; Wang, B.; Yue, Z.; Yao, B.; Xie, Z.; Cheng, Y.; Wang, L.; Jing, X.; Wang, F. *Angew. Chem., Int. Ed.* **2009**, *48*, 6664−6666.
(8) Ding, J.; Gao, J.; Cheng, Y.; Xie, Z.; Wang, L.; Ma, D.; Jing, X.; Wang, F. *Adv. Funct. Mater.* **2006**, *16*, 575−581.
(9) Anthopoulos, T. D.; Frampton, M. J.; Namdas, E. B.; Burn, P. L.; Samuel, I. D. W. *Adv. Mater.* **2004**, *16*, 557−560.
(10) Xia, D.; Wang, B.; Chen, B.; Wang, S.; Zhang, B.; Ding, J.; Wang, L.; Jing, X.; Wang, F. *Angew. Chem., Int. Ed.* **2014**, *53*, 1048−1052.
(11) Lo, S.-C.; Richards, G. J.; Markham, J. P. J.; Namdas, E. B.; Sharma, S.; Burn, P. L.; Samuel, I. D. W. *Adv. Funct. Mater.* **2005**, *15*, 1451−1458.
(12) Lo, S.-C.; Bera, R. N.; Harding, R. E.; Burn, P. L.; Samuel, I. D. W. *Adv. Funct. Mater.* **2008**, *18*, 3080−3090.
(13) Lo, S.-C.; Harding, R. E.; Shipley, C. P.; Stevenson, S. G.; Burn, P. L.; Samuel, I. D. W. *J. Am. Chem. Soc.* **2009**, *131*, 16681−16688.
(14) Baldo, M. A.; Forrest, S. R. *Phys. Rev. B: Condens. Matter Mater. Phys.* **2000**, *62*, 10958−10966.
(15) Baldo, M. A.; Adachi, C.; Forrest, S. R. *Phys. Rev. B: Condens. Matter Mater. Phys.* **2000**, *62*, 10967−10977.
(16) Qin, T.; Ding, J.; Wang, L.; Baumgarten, M.; Zhou, G.; Müllen, K. *J. Am. Chem. Soc.* **2009**, *131*, 14329−14336.
(17) Li, Y.; Liu, Y.; Zhou, M. *Dalton Trans.* **2012**, *41*, 2582−2591.
(18) Cho, Y.-J.; Wee, K.-R.; Son, H.-J.; Cho, D. W.; Kang, S. O. *Phys. Chem. Chem. Phys.* **2014**, *16*, 4510−4521.
(19) Kwon, T.-H.; Kim, M. K.; Kwon, J.; Shin, D.-Y.; Park, S. J.; Lee, C.-L.; Kim, J.-J.; Hong, J.-I. *Chem. Mater.* **2007**, *19*, 3673−3680.
(20) Zhou, G.; Wong, W.-Y.; Yao, B.; Xie, Z.; Wang, L. *Angew. Chem., Int. Ed.* **2007**, *46*, 1149−1151.
(21) Liang, B.; Hu, S.; Liu, Y.; Fan, Z.; Wang, X.; Zhu, W.; Wu, H.; Cao, Y. *Dyes Pigm.* **2013**, *99*, 41−51.
(22) Namdas, E. B.; Anthopoulos, T. D.; Samuel, I. D. W.; Frampton, M. J.; Lo, S.-C.; Burn, P. L. *Appl. Phys. Lett.* **2005**, *86*, 161104.
(23) Frampton, M. J.; Namdas, E. B.; Lo, S.-C.; Burn, P. L.; Samuel, I. D. W. *J. Mater. Chem.* **2004**, *14*, 2881−2888.
(24) Finkenzeller, W. J.; Hofbeck, T.; Thompson, M. E.; Yersin, H. *Inorg. Chem.* **2007**, *46*, 5076−5083.
(25) Rai, V. K.; Nishiura, M.; Takimoto, M.; Hou, Z. *J. Mater. Chem. C* **2013**, *1*, 677−689.
(26) Wasserberg, D.; Meskers, S. C. J.; Janssen, R. A. J. *J. Phys. Chem. A* **2007**, *111*, 1381−1388.
(27) Kawamura, Y.; Goushi, K.; Brooks, J.; Brown, J. J.; Sasabe, H.; Adachi, C. *Appl. Phys. Lett.* **2005**, *86*, 071104.
(28) Li, X.; Chen, Z.; Zhao, Q.; Shen, L.; Li, F.; Yi, T.; Cao, Y.; Huang, C. *Inorg. Chem.* **2007**, *46*, 5518−5527.
(29) Maiorano, V.; Perrone, E.; Carallo, S.; Biasco, A.; Pompa, P. P.; Cingolani, R.; Croce, A.; Blyth, R. I. R.; Thompson, J. *Synth. Met.* **2005**, *151*, 147−151.
(30) Jung, K. M.; Kim, K. H.; Jin, J. I.; Cho, M. H.; Choi, D. H. *J. Polym. Sci., Polym. Chem.* **2008**, *46*, 7517−7533.
(31) Lamansky, S.; Djurovich, P.; Murphy, D.; Abdel-Razzaq, F.; Lee, H. E.; Adachi, C.; Burrows, P. E.; Forrest, S. R.; Thompson, M. E. *J. Am. Chem. Soc.* **2001**, *123*, 4304−4312.
(32) Hwang, A.-R.; Han, W.-S.; Wee, K.-R.; Kim, H. Y.; Cho, D. W.; Min, B. K.; Nam, S. W.; Pac, C.; Kang, S. O. *J. Phys. Chem. C* **2012**, *116*, 1973−1986.
(33) Platt, J. R. *J. Chem. Phys.* **1949**, *17*, 484−495.
(34) Johnson, G. E. *J. Phys. Chem.* **1974**, *78*, 1512−1521.
(35) Thomas, K. R. J.; Thompson, A. L.; Sivakumar, A. V.; Bardeen, C. J.; Thayumanavan, S. *J. Am. Chem. Soc.* **2005**, *127*, 373−383.
(36) Varnavski, O.; Samuel, I. D. W.; Pàlsson, L.-O.; Beavington, R.; Burn, P. L.; Goodson, T., III. *J. Chem. Phys.* **2002**, *116*, 8893−8903.
(37) Devadoss, C.; Bharathi, P.; Moore, J. S. *J. Am. Chem. Soc.* **1996**, *118*, 9635−9644.
(38) Förster, T. *Ann. Phys. (Leipzig)* **1948**, *2*, 55−75.
(39) Stewart, J. J. P. *J. Comput. Chem.* **1989**, *10*, 209−220.